 doi:10.20944/preprints202210.0115.v1

Article

Characteristics of the Fracture Process Zone for Reservoir Rock with Various Heterogeneity

Hongran Chen [1, 2], Jingrui Niu [3,*] and Mengyang Zhai [1, 2]

[1] Key Laboratory of Shale Gas and Geoengineering, Institute of Geology and Geophysics, Chinese Academy of Sciences, Beijing 100029, China; chenhongran@mail.iggcas.ac.cn
[2] Innovation Academy for Earth Science, CAS, Beijing 100029, China; chenhongran@mail.iggcas.ac.cn
[3] Chinese Society for Rock Mechanics and Engineering, Beijing 100029, China; niujingrui@mail.iggcas.ac.cn
* Correspondence: niujingrui@mail.iggcas.ac.cn

Abstract: Hydraulic fracturing for oil-gas and geothermal reservoir stimulation is closely related to the generation and propagation of Mode I crack. Nonlinear deformation due to rock heterogeneity occurs at such crack tip, which causes the fracture process zone (FPZ) to form before the crack propagates unsteadily. However, the relationship between the FPZ characteristics and rock heterogeneity still remain elusive. We used three rock types common in reservoir for experimental investigation, and each of them includes two subtypes with different heterogeneity due to grain size or microstructural characteristics. Drawing on the experiment results, we calculated the FPZ size in each cracked chevron notched Brazilian disk, and we reproduced the formation process of the FPZ in marble by discrete element method. We showed that strong heterogeneity is favorable to large FPZ size, can enhance the ability of crack generation and complicate crack morphology. Coupling the Weibull distribution with fracture mechanics, the dependence of the FPZ size on heterogeneity degree can be theoretically explained, which suggests that inherent heterogeneity of rocks set physical foundation for formation of FPZ. These findings can improve our recognition to formation mechanism of the Mode I crack and provide useful guidelines for evaluating reservoir fracability.

Keywords: Mode I crack; fracture process zone; heterogeneity; discrete element method; reservoir fracability

1. Introduction

Hydraulic fracturing is extensively used to stimulate oil-gas and geothermal reservoir. This technique involves the generation and propagation of cracks within strata driven by injected fluids. The majority of the hydraulic cracks can be viewed as Mode I cracks as fracture mechanics defined [1], because fluid pressures imposing on crack surfaces are equivalent to remote tensions in nature. Therefore, the propagation mechanism of Mode I crack is a significant fundamental subject for raising conductivity of fracture networks by hydraulic fracturing.

Natural rocks usually contain various microscopic structures, such as mineral grain boundaries, cleavages, pores and cracks [2]. Compared to mineral crystal, these structures are local weak zones in rocks, because stress concentration arise at the vicinity of their tips, which cause preexisting cracks to propagation and new cracks to grow. Furthermore, various mineral grains constituting rocks usually have distinct mechanical properties, and the contacts between grains can be also different. Lan *et al.* [3] referred to these terms of heterogeneity as geometric, elastic and contact heterogeneities. These properties make the distribution of mesoscopic strength in rocks heterogeneous, and micro cracking will initiate from tips of microstructures [4]. Micro cracks arising around the tips connect and coalesce progressively with imposed load increasing, forming macroscopic cracks and causing them to propagate in an unstable manner, i.e., spontaneous propagation under unchanged load. Such a zone at a crack tip in which many micro cracks grow is called fracture process zone (FPZ) [5]. The formation of FPZs represent the preparation process for

Preprints (www.preprints.org) | NOT PEER-REVIEWED | Posted: 10 October 2022 doi:10.20944/preprints202210.0115.v1

the unstable crack propagation and indicate the nonlinear rocks deformation. Size of the FPZs suggest the degree of the nonlinearity, and thereby is one of the most critical parameters for characterizing the cracking behavior of rocks.

To this end, quite a few researchers have investigated the effect of various factors on the FPZ size. For example, Labuz *et al.* [6] observed that FPZs in Rockville granite (average grain size 10mm) were longer than those in Charcoal granite (average grain size 1mm) during double-cantilever-beam tests. Moazzami *et al.* [7] reported that the FPZ size differs across lithology, which may be also related to different grain size. Zietlow and Labuz [8] proposed an approximately linear relation between the width of FPZ and the logarithm of the grain size. These studies suggest that FPZ size can be positively related to grain size; and this speculation is consolidated by the nanoscale observation [9]. The scale effect of specimen on the FPZ size is similar to the effect of grain size: the FPZ size was observed to grow with the scale of specimens increasing in both single edge notch bending and semi-circular bend tests [7,10,11].

Haidar *et al.* [12] found that the existence of pores caused the distribution regions of acoustic emission (AE) events in front of notch tips (i.e., FPZs) to extend. Guha Roy *et al.* [13] investigated the effect of joints and showed a negative correlation between the FPZ size and joint spacing. Therefore, the importance of microstructures to the FPZ size have been recognized.

The aforementioned research revealed that the FPZ size is highly dependent on the physical, geometrical and structural properties of rocks. In fact, these properties can be associated with heterogeneity: grain size and microstructure can influence the strength spatial distribution within rocks; and large specimens usually contain more microstructures. Researchers [14-16] have pointed out that the heterogeneity of reservoir rocks make impacts on its fracability, i.e., the possibility for reservoirs to create adequate fractures permitting fluids transportation. For example, Yang *et al.* [16] stated that the hydraulic fracture path becomes smooth as the heterogeneity degree of reservoir decreases, which is unfavorable to connecting pores and natural preexisting cracks. Reliable fracability evaluation is critical to hydraulic fracturing design; considering that both the FPZ size and fracability rely on reservoir heterogeneity, the former may be useful to evaluate the latter.

However, yet the relationship between the FPZ size and heterogeneity has not been clarified. We will analyze the effect of heterogeneity on the FPZ size using experiment, numerical simulation and mechanical analysis. The expected findings can improve our understanding of the essential mechanism of the FPZ formation and help to evaluate fracability more reliably.

2. Materials and Methods

2.1. Lithology, structural characteristics and heterogeneity

We purchased marble, limestone and shale from the construction material market in Beijing, China for the experimental investigations. Marble was reported to compose certain geothermal reservoirs [17], and limestone and shale are common lithology serving as conventional and unconventional oil-gas reservoirs. Therefore, engineering implications in energy resources exploitation can be acquired from the research on these rock types.

The marble includes subtypes J and K. Both of them consists of calcite, and their average grain size are 1–2 mm and 2–4 mm (Fig. 1a and 1b), respectively. The marble K is more heterogeneous because larger grains usually have lower boundary cohesion [18], which results in significant differences of strength between grains and contacts.

The limestone can be divided into subtypes P and N according to the characteristics of the ooid. The limestone P contains homogeneous ooid whose size is closed to 2 mm (Fig. 1c). The ooid size of N falls in the range of 1–5 mm, and coarse calcite grains are observed in the cryptocrystalline matrix (Fig. 1d). The ooid in the N are in dark color and thus more visible than those in the P (Figs. 1c and 1d), which may suggest the more considerable differences of physical properties between the ooid and matrix. In addition, the ooid size of the N has a wider range that corresponds to a heterogeneous size distribution.

Preprints (www.preprints.org) | NOT PEER-REVIEWED | Posted: 10 October 2022 doi:10.20944/preprints202210.0115.v1

The coarse calcite grains also enhance the heterogeneity. For these reasons, the limestone N is more heterogeneous than P.

The shale can be divided into subtypes S_1 and S_2 owing to their different characteristics of mineral distribution. The shale S_1 and S_2 consists of white and green minerals (their major compositions acquired by X-ray diffraction (XRD) analysis are shown in Table 1). White minerals scatter homogeneously in each layer of S_1, mixing with green minerals (Fig. 1e), whereas white and green layers are alternative in S_2 (Fig. 1f); therefore, S_2 is more heterogeneous than S_1.

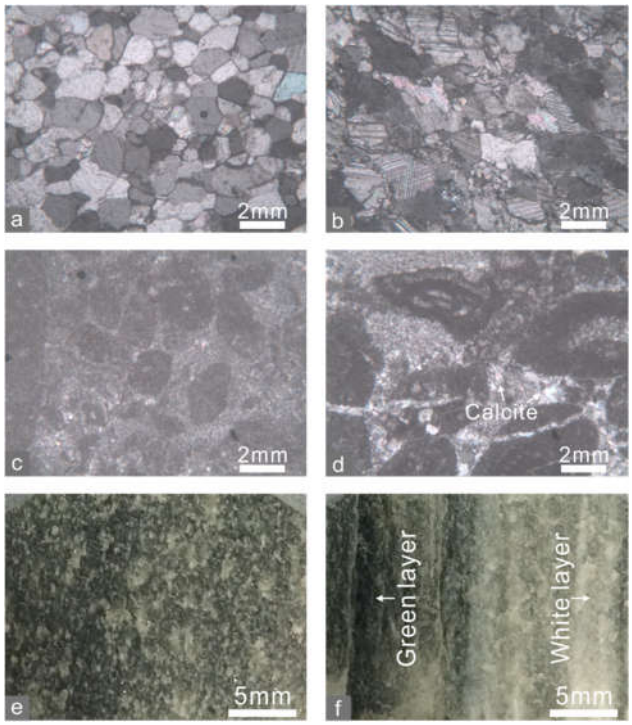

Figure 1. Microstructures of the marble (a) J, (b) K, limestone (c) P and (d) N and different characteristics of mineral distribution in the shale (e) S_1 and (f) S_2.

Table 1. XRD results of the shale

Sample	Quartz (%)	Orthoclase (%)	Plagioclase (%)	Calcite (%)	Clay (%)
S_1	48.2	/	17.2	13.9	20.7
S_2 (green layer)	19.9	1.5	4.1	55.3	19.2
S_2 (white layer)	16.4	/	/	81.8	1.8

2.2 Measurement method of the FPZ size

The FPZ size can be measured directly during or after rock mechanical experiments using various techniques, e.g., AE monitoring [19] and digital image correlation [20]. These methods are usually limited to relatively intact and large specimens so that sensors can be set to carry out observation. However, such specimens can be difficult to obtain using slim cores collected from exploring wells. Another measurement method is to calculate the FPZ size based on certain parameters measured by experiments [21]. The general expression of the FPZ size r is as follows [1]:

$$r = \alpha \left(\frac{K_{IC}}{\sigma_Y}\right)^2, \quad (1)$$

where K_{IC} is the Mode I fracture toughness, σ_Y is the yield strength, and α is a coefficient related to specimen geometry. The σ_Y is determined by yield criterion: the Mises and Tresca criteria suit for metal, while maximum tensile strength criterion is widely used for rocks, because the yield strength σ_Y of rocks in tension often lies close to their tensile

Preprints (www.preprints.org) | NOT PEER-REVIEWED | Posted: 10 October 2022 doi:10.20944/preprints202210.0115.v1

strength σ_t [9]. Based on this criterion, the FPZ is a circular region that is centered by the crack tip; and thus the calculation formula of the FPZ size (i.e., the circle radius) [5] is

$$r = \frac{1}{2\pi}\left(\frac{K_{IC}}{\sigma_t}\right)^2. \quad (2)$$

Considering its convenience and reliability [9], we use this method to measure the FPZ size.

2.3 Measurement methods of tensile strength and Mode I fracture toughness

The calculation of the FPZ size using Eq. (2) requires the tensile strength and Mode I fracture toughness of rocks measured by experiments. Brazilian disk (BD) test that International Society for Rock Mechanics (ISRM) [22] and American Society for Testing Materials (ASTM) [23] recommend is the most extensively used method for measuring tensile strength of rocks. Referring to the suggestion from ASTM [23] that the range of thickness (B)-to-diameter (D) ratio is 0.2–0.75 and the diameter of BD specimens should be larger than 50 mm, the BD specimens is set to be 75 mm in diameter and 30 mm in thickness (Fig. 2a). Each BD test was performed at a constant displacement rate of 0.06 mm/min by an MTS servo-control testing machine (series CMT) until the applied axial load attains its maximum (P_{max}) and the specimen ruptured. The tensile strength (σ_t) is calculated by

$$\sigma_t = \frac{2P_{max}}{\pi BD}. \quad (3)$$

BD tests were conducted on at least three specimens in parallel with the same lithology, and the average strength was taken as the tensile strength of the rock type.

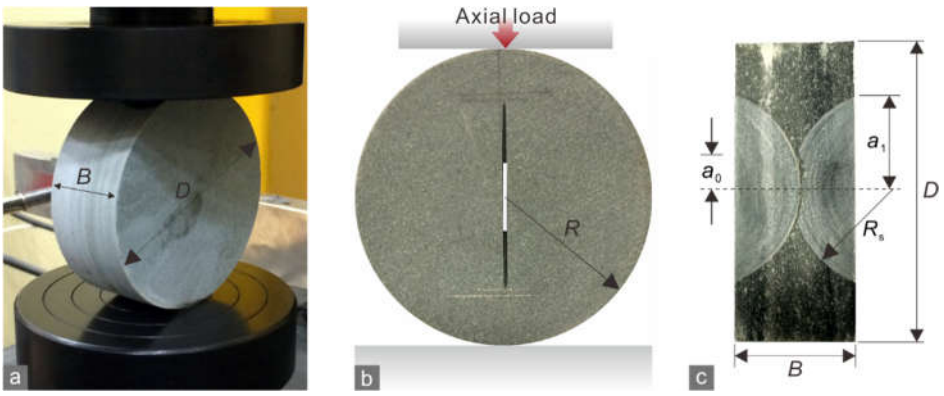

Figure 2. (a) An ongoing BD test on shale. Thickness B = 30mm and diameter D = 75mm. (b) Orthographic and (c) side profiles of a CCNBD shale specimen. Geometric parameters: diameter D = 75 mm, radius R = 37.5 mm, thickness B = 30 mm, saw radius R_s = 25 mm, initial chevron notched crack length a_0 = 8.45 mm, and final chevron notched crack length a_1 = 23.5 mm. Dimensionless parameters: $\alpha_0 = a_0 / R$, $\alpha_1 = a_1 / R$, and $\alpha_B = B / R$.

The Mode I fracture toughness of rocks can be measured using several methods [24-26] as the ISRM recommended, including chevron notched three-points round bar, chevron notched short rod, semi-circular bend and cracked chevron notched Brazilian disk (CCNBD). We used the CCNBD test because it gives out stable and reliable results. What is more important, CCNBD specimens have similar boundary conditions and geometry to BD specimens, which can eliminate the effects of loading conditions and size as much as possible.

Preprints (www.preprints.org) | NOT PEER-REVIEWED | Posted: 10 October 2022 doi:10.20944/preprints202210.0115.v1

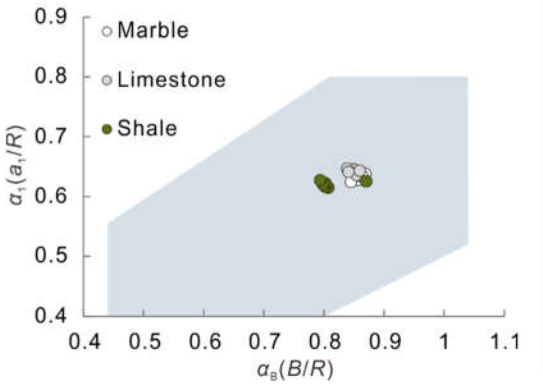

Figure 3. Valid range for parameters α_1 and α_B (blue shadow, [26]) and the distribution of parameter values for all of the prepared CCNBD specimens.

The notched crack of each CCNBD specimen was created by a circular diamond saw. The actual values of the geometric parameters (shown in Fig. 2b and 2c) were measured to confirm that the dimensionless parameters α_1 and α_B of all CCNBD specimens fall within the valid range (Fig. 3). The procedure of CCNBD test is identical to those of BD test, adopting the same experimental apparatus.

According to [26], the Mode I fracture toughness K_{IC} can be calculated using this formula:

$$K_{IC} = \frac{P_{max} Y^*_{min}}{B\sqrt{R}}, \quad (4)$$

where P_{max} is the maximum axial load applied in the test, Y^*_{min} is the critical dimensionless stress intensity value, and R is the disk radius. Y^*_{min} is determined by

$$Y^*_{min} = ue^{v\alpha_1}, \quad (5)$$

where u and v are constants that are determined by α_0 and α_B [26].

2.4 Discrete element method (DEM) and grain-based model

We used Particle Flow Code in Two Dimensions (PFC2D), a popular commercial code drawing on discrete element method (DEM) to reproduce the experimental results. The PFC2D is based on the bonded-particle assumption [27] that rock is represented by an assembly of inter-bonded circular particles. The mechanical behavior of rock is dominated by the microscale properties and constitutive relations of the bonded contacts between the particles. When a component of the contact force in the normal and shear directions attains the tensile or shear bond strength, the successive breakage of bonds viewed as crack propagation occurs.

The primary drawback of conventional PFC2D is the lack of consideration of grain structures. However, crystalline rocks usually contain polygonal minerals, of which the microstructure including grain shape and size can strongly influence the mechanical behaviors [28]. To address this issue, a grain-based model (GBM) with polygon-tessellation grain boundaries taking grain breakage into account has been implemented in PFC2D [29,30]. Using the DEM with GBM modeling, we simulated the experimental results for marble J and K.

To implement the GBM of marble, an initial particle aggregate with a particle size distribution consistent with observations is created firstly (Fig. 4a), and then we develop Voronoi-tessellation mineral boundaries along the particle boundaries (Fig. 4b). Next, the larger particles of the initial aggregate will be replaced by smaller circular particles (Fig. 4c). Finally, soft-bonded (Fig. 5a) and smooth-joint models (Fig. 5b) expressing bonded and unbonded behaviors are assigned on intra-grain and inter-grain contacts, respectively (Fig. 4d).

Preprints (www.preprints.org) | NOT PEER-REVIEWED | Posted: 10 October 2022 doi:10.20944/preprints202210.0115.v1

The recent developed soft-bonded model [31] is a more reliable one to characterize intra-grain contact because the strain-softening property of the bonds is considered [32]. When the bond tensile strength is attained, the bond failure displays a softening regime (Fig. 6a), i.e., the bond force in its normal direction declines, causing breakage, and then the contact shifts to unbonded state (Fig. 6b). In the unbonded state a force and moment can be transmitted at the contact point, and the contact provides frictional force resisting sliding.

The smooth-joint contacts [33] are assigned on the two sides of a grain boundary, removing the previous bonds. The orientation of the contacts is parallel to the boundary. Once the bonds break, their behavior changes to friction. This contact model allows the overlapping of particles in unbonded state (Fig. 5b).

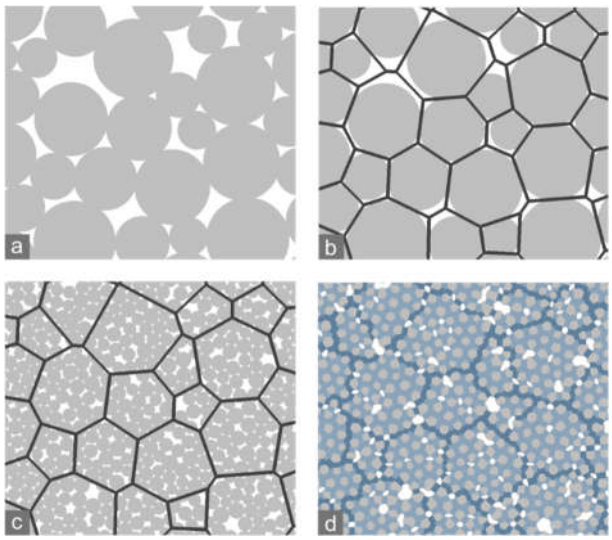

Figure 4. Modeling of GBM for marble. Grey circles are particles, and black lines define the polygonal minerals in (b) and (c). The light and dark blue curves in (d) denote intra- and inter-grain contacts.

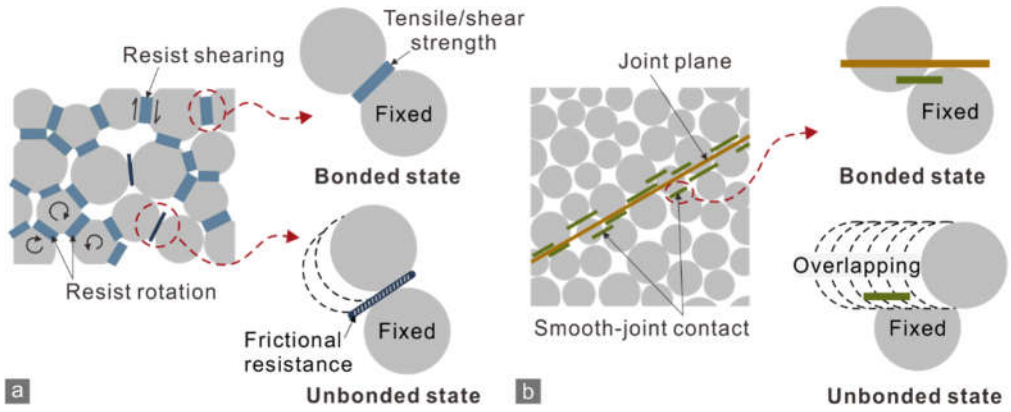

Figure 5. Schematic of bonded and unbonded state for (a) soft-bonded and (d) smooth-joint models.

Preprints (www.preprints.org) | NOT PEER-REVIEWED | Posted: 10 October 2022 doi:10.20944/preprints202210.0115.v1

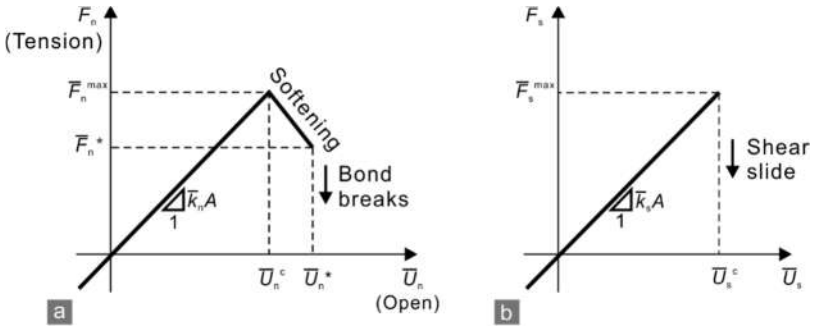

Figure 6. Force–displacement relationship of soft-bonded contact in (a) bonded [32] and (b) unbonded state. $\bar{F}_n$: normal force; $\bar{F}_n^{max}$: peak normal force; $\bar{F}_n^*$: normal force corresponding to bond breakage; $\bar{F}_s$: tangential shear force; $\bar{F}_s^{max}$: peak tangential shear force; $\bar{U}_n$: normal displacement; $\bar{U}_n^c$: normal displacement corresponding to peak normal force; $\bar{U}_n^*$: normal displacement corresponding to bond breakage; $\bar{U}_s^c$: tangential displacement corresponding to onset of shear slide; $\bar{k}_n$: normal stiffness; $\bar{k}_s$: tangential stiffness; A: cross-sectional area.

2.5 Model setup and parameter calibration

Four GBMs were created to simulate the BD and CCNBD tests on marble J and K specimens. Each model comprised ~20,000 circular particles with a 0.2–0.3 mm radius. The GBMs were positioned between two stiff walls representing the loading end and platform of a compression machine, and the walls moved toward each other at the same constant velocity to result in a quasi-static loading rate.

The BD test results were used to calibrate the microscale parameters of the particles and intra- and inter-grain contacts. The approximate values of these parameters were determined referring to the elastic properties of calcite [34] and the previous work [35], and then the calibration was achieved iteratively through trial and error [30]. When the simulated load–displacement curves and crack morphology fitted well with the observations in the BD tests (Fig. 7), the rationality of the adopted microscale parameters (Table 2) was confirmed. Thus, the simulation results of CCNBD test based on the calibrated parameters can be reliable.

Table 2. Calibrated microscale parameters of marble J and K

Elements	Microscale parameter	Marble J	Marble K
Particles	Density (kg/m^3)	2690	2690
	Effective modulus (GPa)	70	70
	Normal to shear stiffness ratio	1.5	1.5
	Friction coefficient	0.6	0.6
Soft-bonded intra-grain contact	Effective modulus (GPa)	10.0	15.0
	Normal to shear stiffness ratio	2.0	2.0
	Friction coefficient	0.6	0.6
	Tensile strength (MPa)	18.0	37.5
	Cohesion (MPa)	72.0	150.0
	Friction angle (°)	45	45
	Softening factor	0.1	0.1
	Softening tensile strength factor	0.7	0.7
Smooth-joint inter-grain contact	Tensile strength coefficient	0.3	0.3
	Cohesion coefficient	0.8	0.8
	Friction angle coefficient	0.6	0.6
	Friction adjustment coefficient	0.5	0.5
	Normal stiffness coefficient	0.8	0.8
	Shear stiffness coefficient	0.15	0.15

Preprints (www.preprints.org) | NOT PEER-REVIEWED | Posted: 10 October 2022 doi:10.20944/preprints202210.0115.v1

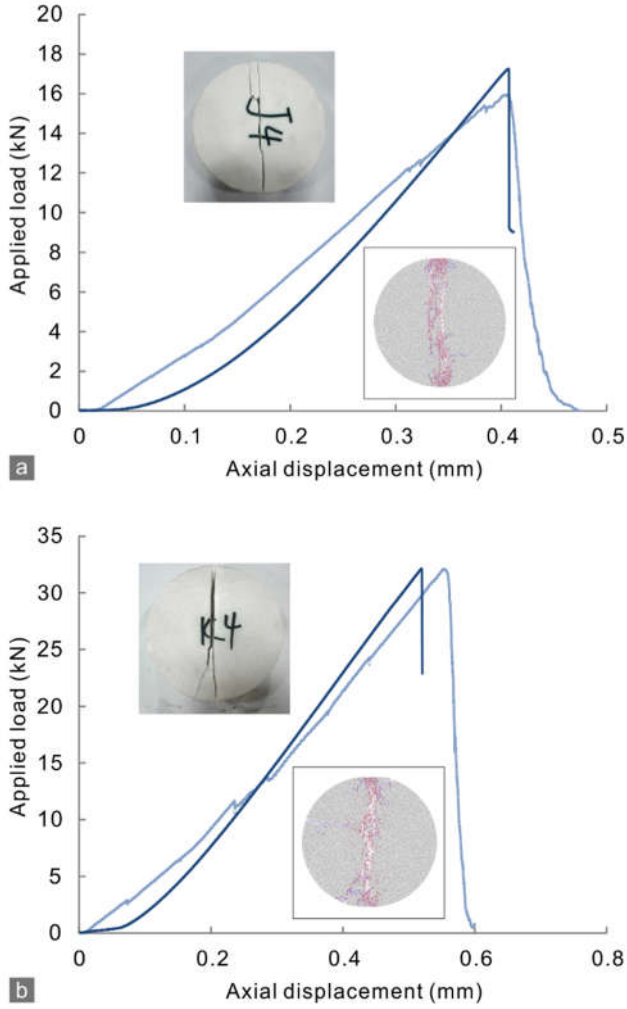

Figure 7. Load–displacement relationship of experimental (dark blue curves) and numerical (light blue curves) results for (a) marble J and (b) K in the BD test and the corresponding fracture morphology.

3. Results

3.1. The tensile strength, fracture toughness and FPZ size

The tensile strength and Mode I fracture toughness did not exhibit consistent correlation with heterogeneity of the rocks (Fig. 8a and 8b). The more heterogeneous N has the greater tensile strength and fracture toughness than P, whereas the values of these properties of S_2 is smaller than those of relatively homogeneous S_1.

The more heterogeneous subtypes of the marble, limestone and shale (K, N and S_2) generated larger FPZs than the relatively homogeneous subtypes (J, P and S_1) did (Fig. 8c). The increasing trend of the FPZ size with the rising degree of heterogeneity of rocks suggests that strong heterogeneity is favorable to form larger FPZ. The variation trend of the FPZ size with rock types with different heterogeneity is not consistent to those of the tensile strength and fracture toughness (Fig. 8), indicating that the FPZ size is neither dependent on the former nor the latter properties.

The present and previous experiment results [36] showed that the tensile strength and fracture toughness displayed a positive linear correlation (Fig. 9), which indicates that the ratios of the two properties change within a narrow range.

Preprints (www.preprints.org) | NOT PEER-REVIEWED | Posted: 10 October 2022 doi:10.20944/preprints202210.0115.v1

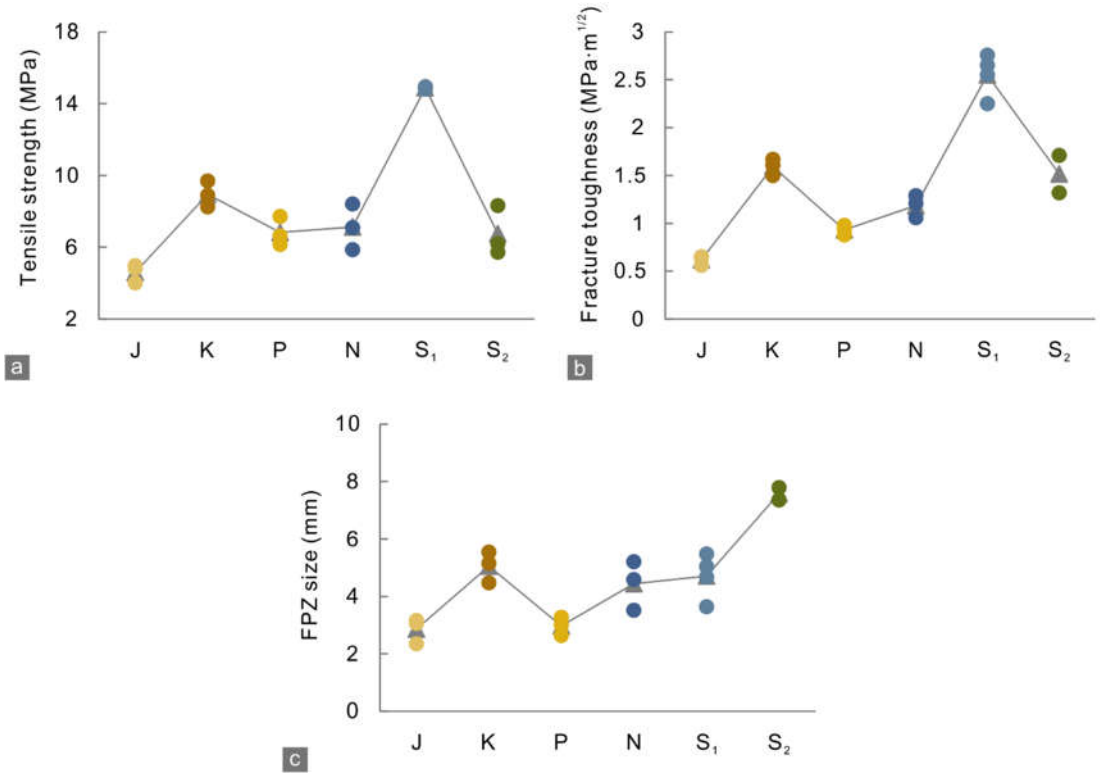

Figure 8. (a) Tensile strength, (b) Mode I fracture toughness and (c) FPZ size of the six rock types. Grey triangles mean averages.

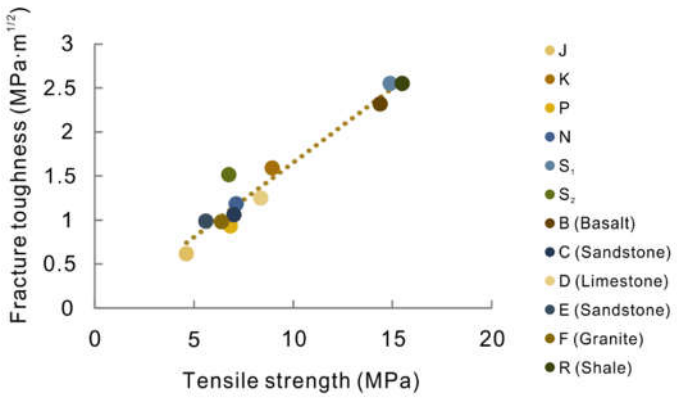

Figure 9. Linear correlation between the tensile strength and fracture toughness. The data of rocks B–F and R refer to [36].

3.2 Crack morphology

The specimens of the subtypes with stronger heterogeneity and larger FPZ size generated more curving, irregular even branched cracks with great apertures (Fig. 10). Some of these specimens were dramatically broken into several parts soon after the macroscopic rupture occurs, resulting in relatively rough cracking surfaces with quite a few fragments and powders. That is, the larger FPZ size correspond to the more complex morphology of cracks.

White patches were notable in front of the notched crack tips on surface of the marble K specimens (Fig. 10b). Such patches, which were commonly observed on crystalline rock (e.g., marble [37] and granite [38]) with medium or coarse grain size, were attributed to high-density micro cracks and indicated that the FPZ size was considerable enough to be visible.

In contrast, the less heterogeneous rock specimens generate relative straight cracks with small apertures (Fig. 10). Especially, no discernible white patches indicating FPZ

Preprints (www.preprints.org) | NOT PEER-REVIEWED | Posted: 10 October 2022 doi:10.20944/preprints202210.0115.v1

were observed in the relatively homogeneous marble J specimens when the imposed loads approach to the maximums (Fig. 10a) because of their smaller FPZ size.

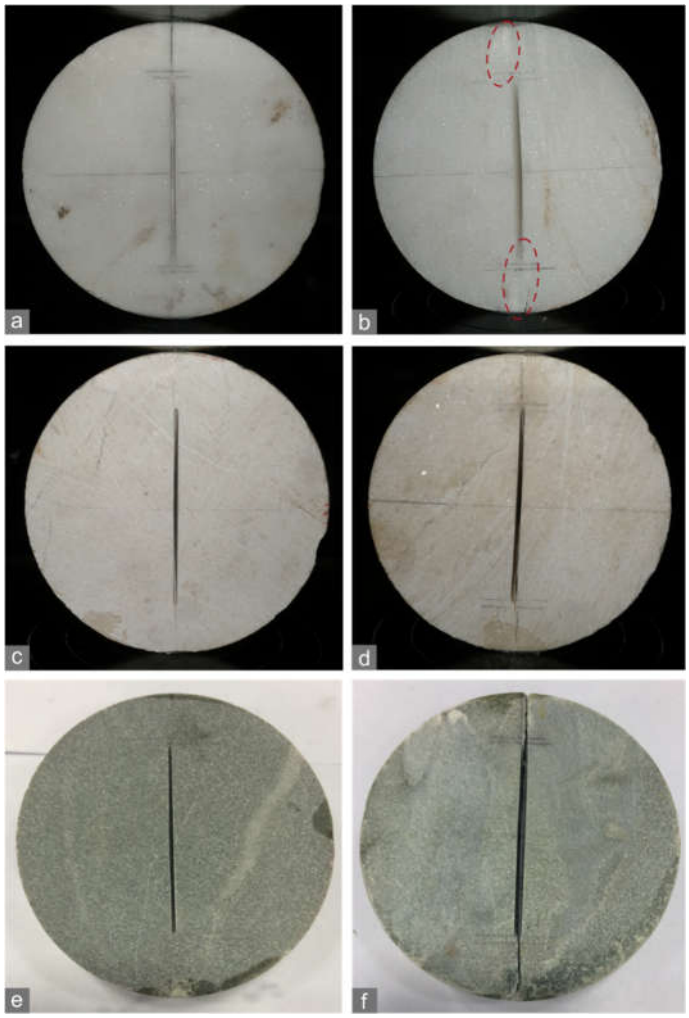

Figure 10. Crack path and aperture observed in the CCNBD specimens of the (a) marble J, (b) marble K, (c) limestone P, (d) limestone N, (e) shale S_1, and (f) shale S_2. Dashed circles in (b) denote the white patches indicating FPZs.

3.3 Characteristics of the FPZ in DEM models for the marble

The DEM simulations showed that the marble J and K specimens had similar formation process of FPZ (Fig. 11). Micro cracks initiate around the two notched crack tips in each specimen owing to strong stress concentration. As the applied load increases, they gradually grow along the direction approximately parallel to the strike of the notched crack, and the number rises at a relatively stable rate. When the density of micro cracks is high enough to form macroscopic cracks, the growth rate of micro crack begins to accelerate dramatically. Once the load reaches its peak value, the size of the FPZ will also reach its maximum, and then the macroscopic cracks will propagate catastrophically and cross the whole specimen, which results in the rupture of the specimen characterized by a sharp post-peak stress drop, because they connect with those micro cracks initiating from the point that a specimen contacts with the loading end (or platform). When the load drops to an approximately constant level corresponding to residual strength of specimen, the whole loading process terminates.

The normalized load levels corresponding to the initiation and acceleration onset of micro crack growth are quite different for the two marble subtypes (Fig. 11). Initiation and acceleration of micro crack growth arises respectively at ~50%P_{max} and ~90%P_{max} in the marble K, which are lower than those levels in the marble J (~70%P_{max} and ~95%P_{max}). In

Preprints (www.preprints.org) | NOT PEER-REVIEWED | Posted: 10 October 2022 doi:10.20944/preprints202210.0115.v1

other words, crack growth occurred earlier (i.e., more easily) in the marble K than it did in the marble J, although the former has higher strength. Furthermore, the marble K also generated more micro cracks than the marble J did. J and K specimens generated 345 and 624 micro cracks during their pre-peak stages; and the total number of micro cracks generated within their whole loading processes are 1404 and 1588. For the same reason, more zigzags (due to local drops of load representing crack generation) were visible on the displacement–load curve of the marble K, which suggest stronger non-linearity of deformation.

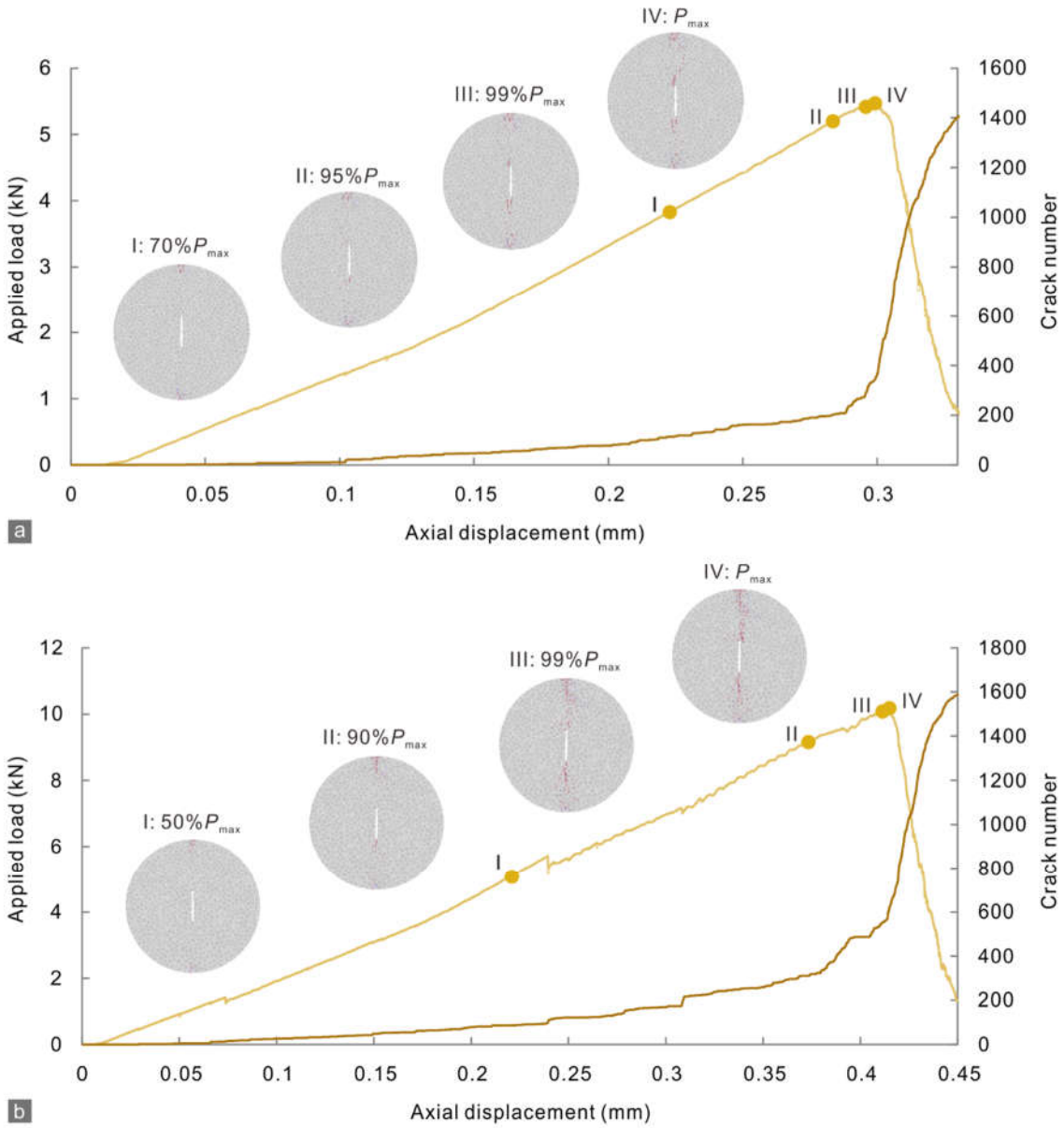

Figure 11. Applied load and crack number vs. axial displacement relationship for (a) marble J and (b) K in the simulated CCNBD test and the fracture morphology corresponding to certain levels of applied load. Points I: micro cracks growth from notched crack tips; II: onset of accelerated growth of micro crack; III: formation of macroscopic crack; IV: peak-load point with the FPZ size reaching its maximum.

Consistent with the above results of micro crack number, the crack distribution range in the marble K specimen is larger than that in the marble J specimen when the specimens were loaded to attain their peak-load points (Fig. 11), suggesting greater size (especially the length) of the FPZ.

Preprints (www.preprints.org) | NOT PEER-REVIEWED | Posted: 10 October 2022 doi:10.20944/preprints202210.0115.v1

To conduct more quantitive investigation on the morphology of the FPZ, we defined a 7 × 7mm² study area at each notched crack tip that consists of 1 × 1mm² observation windows and count the crack number within each window. The crack density at a notched crack tip is usually relatively high, defining the core zone of a FPZ, and the density gradually decreases to a low background level as the distance from the tip in either X or Y direction increases (Fig. 12). We viewed that the background density of micro crack in the DEM models as ≤2/mm² because this density level representing minor non-linear deformation was reached in the early loading stage. In this context, the maximum length of FPZs of the marble J and K are 5mm and 7mm, and their maximum width are 3mm and 4mm. That is, the marble K with stronger heterogeneity generated a larger FPZ. This trend agrees to the experimental results, which further confirms the reliability of the DEM simulations.

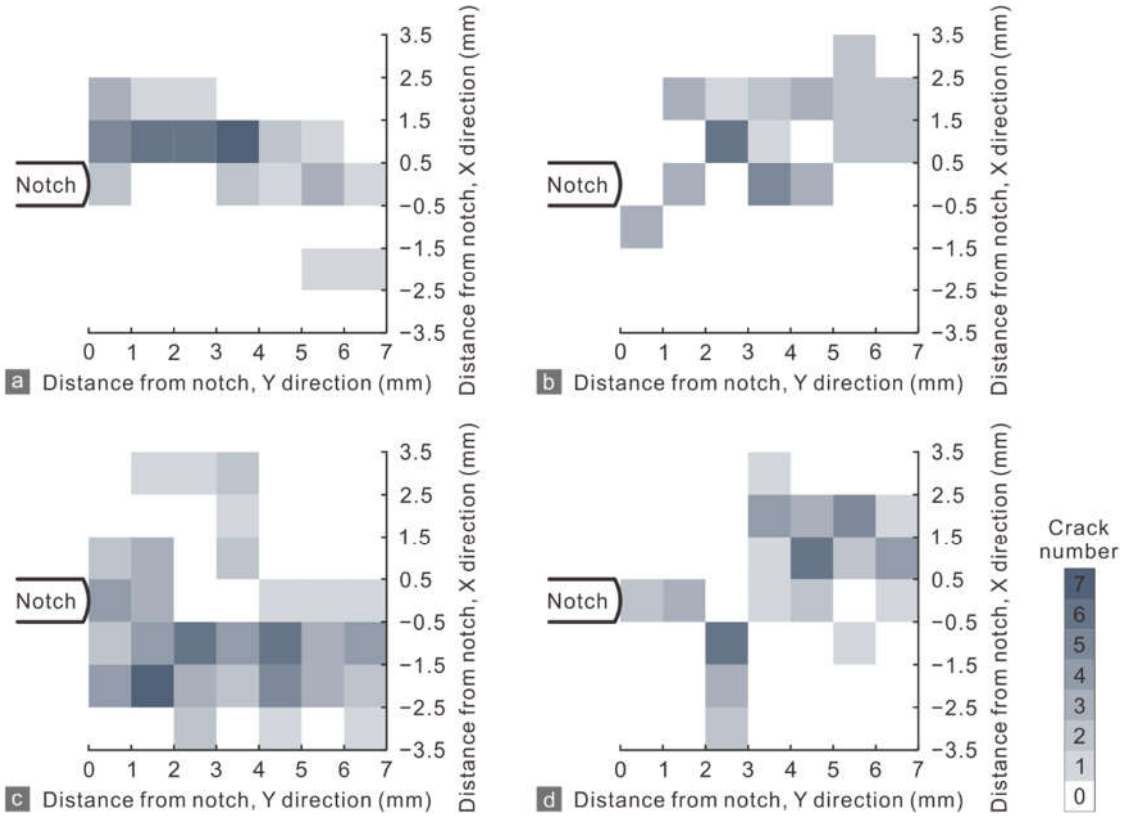

Figure 12. Micro crack number distribution within study areas (7 × 7mm²) at the vicinity of the upper and lower notched crack tips of (a)–(b) marble J and (c)–(d) K. X and Y directions are respectively perpendicular and parallel with the strike of the notched crack.

4. Discussion

4.1. Effects of heterogeneity

Heterogeneity suggests that the local strength can differ across areas of a rock specimen. Cracking can occur firstly in the weaker zones, especially when heterogeneity is strong, therefore the marble K showed lower normalized loads that correspond to the initiation and acceleration of micro crack growth. This is because heterogeneous rock with a wider distribution range of local strength is possible to contain more weak zones, which is favorable to micro crack generation. However, such cracking is usually small-scaled and cannot trigger the unstable propagation of macroscopic cracks and the catastrophic rupture of the specimen, because many strong local zones serve as the barriers arresting the small-scale cracking. In this context, unstable propagation requires adequate micro cracks to gather in front of the crack tip, which involves a progressive cracking process and generates a large nonlinear deformation zone, i.e., a FPZ with large size.

Preprints (www.preprints.org) | NOT PEER-REVIEWED | Posted: 10 October 2022 doi:10.20944/preprints202210.0115.v1

Regarding a relative homogeneous rock specimen, local strength in different areas can be similar. Before the applied stress reaches general strength of matrix and microstructures, very few small cracks arise, and thus the FPZ size is small. However, extensive cracking will dramatically occur in the vicinity of the crack tip once the general strength is reached, which causes unstable propagation of macroscopic crack soon after the formation of the FPZ. If a kind of brittle material is totally homogeneous, its deformation will be linear elastic, and thus cracks propagate without any FPZ formation [8]. Therefore, heterogeneity degree of the rock determines the nonlinearity of the deformation at crack tip, and strong heterogeneity corresponds to large FPZ size, as our experiment results revealed. Larger grain size and specimen size and greater number of cracks (pores) can enhance rock heterogeneity [39-41], explaining why these properties can promote the formation of large FPZs. In conclusion, heterogeneity sets the physical foundation for the existence of the FPZ.

Stronger heterogeneity generally suggests more weak zones as sources of cracking; nevertheless, it does not indicate lower tensile strength and fracture toughness, because these two parameters representing the ability to resist deformation and failure rely not only heterogeneity but also the level of general strength.

4.2 Why the FPZ size depends on rock heterogeneity

To clarify the dependence of the FPZ size on heterogeneity, we used a statistical distribution coupling with the theory of fracture mechanics. Rock in the vicinity of a crack tip can be viewed as an aggregation of a certain number of elements that represent various mineral grains or microstructures, therefore these elements have different strengths. Assuming that each element is elastic-brittle and their tensile strengths follow the Weibull distribution [42], the rupture probability P of the elements (i.e., the probability of formation of a macroscopic crack) is

$$P = 1 - \exp\left[-\left(\frac{\sigma}{\sigma_0}\right)^m\right], \tag{6}$$

where σ is the tensile stress, σ_0 is the general tensile strength of the elements, and m is the Weibull modulus. Larger m value indicates that the elements with strengths σ_0 occupy greater proportion of all elements; otherwise, the element strengths can be very different and fall in a wide range. Hence, the parameter m represents the strength heterogeneity of rock and is called heterogeneity index [43,44].

The elements fail as the tensile stress at crack tip increases, thereby raising the failure probability. When the stress reaches σ_0, most elements within the FPZ have failed, indicating the onset of the macroscopic crack propagation (Fig. 13). Therefore, the FPZ forms before the stress reaching σ_0. Provided that rocks with identical σ_0 but different heterogeneity indices m_1 and m_2, we assumed that the FPZ forms when their failure probability reaches P_c:

$$P_c = 1 - \exp\left[-\left(\frac{\sigma_1}{\sigma_0}\right)^{m_1}\right] = 1 - \exp\left[-\left(\frac{\sigma_2}{\sigma_0}\right)^{m_2}\right], \tag{7}$$

where σ_1 and σ_2 ($\sigma_1 < \sigma_0$, $\sigma_2 < \sigma_0$) correspond to FPZ formation. If $m_1 > m_2$ (Fig. 13), we can yield

$$\sigma_1 > \sigma_2, \tag{8}$$

which suggests that small m value (strong heterogeneity) corresponds to the lower stress level that can cause the elements near the crack tip to fail (Fig. 13).

Preprints (www.preprints.org) | NOT PEER-REVIEWED | Posted: 10 October 2022 doi:10.20944/preprints202210.0115.v1

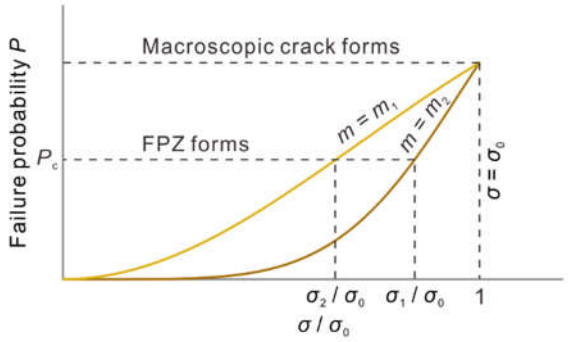

Figure 13. P vs. σ/σ_0 relationship corresponding to different heterogeneity indices m ($m_1 > m_2$) of rock materials.

Based on the assumption that each element is elastic-brittle, the linear elastic fracture mechanics is still valid to describe the stress state at crack tip before unstable propagation. The tensile stress at a Mode I crack tip can be written as

$$\sigma = \frac{K_I}{\sqrt{2\pi r}} \cos\frac{\theta}{2}\left(1 + \sin\frac{\theta}{2}\sin\frac{3}{2}\theta\right), \tag{9}$$

where K_I is the Mode I stress intensity factor, and r and θ are polar coordinate system from the crack tip. Substitute

$$K_I = \sigma^{\infty}\sqrt{\pi a} \tag{10}$$

and $\theta = 0$ into Eq. (9) we obtain

$$\sigma = \sigma^{\infty}\sqrt{\frac{a}{2r}}, \tag{11}$$

where a is the half length of crack, r represents the distance from the crack tip, and σ^{∞} is the remote boundary stress proportional to the general strength σ_0. Eq. (11) gives out the relationship between the σ and r in a certain boundary condition, and the corresponding diagram (Fig. 13) shows that the tensile stress gradually declines with the growing distance from crack tip.

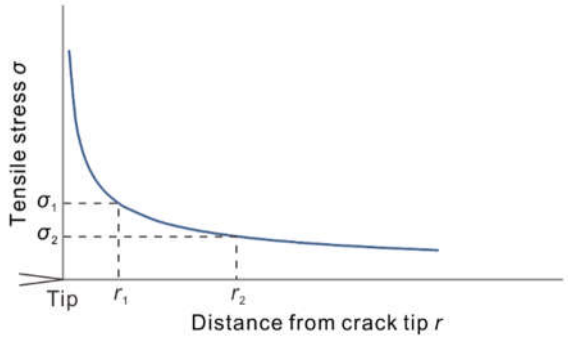

Figure 14. Schematic of the tensile stress distribution in the vicinity of crack tip.

To generate a FPZ with size r, the tensile stress on the FPZ boundary should equal to that corresponds to P_c. Therefore, the aforementioned stress σ_1 and σ_2 can respectively result in two FPZ with size r_1 and r_2, and $r_1 < r_2$. As the Fig. 14 illustrates, the tensile stress within the zones defined by r_1 and r_2 exceeds σ_1 and σ_2, which permit the failed elements within the zones to form the FPZs.

If the rock with identical m value but different general strengths σ_0 and σ_0', Eq. (7) becomes

Preprints (www.preprints.org) | NOT PEER-REVIEWED | Posted: 10 October 2022 doi:10.20944/preprints202210.0115.v1

$$P_c = 1 - \exp\left[-\left(\frac{\sigma_1}{\sigma_0}\right)^m\right] = 1 - \exp\left[-\left(\frac{\sigma_2}{\sigma_0'}\right)^m\right], \quad (12)$$

which yields

$$\frac{\sigma_1}{\sigma_0} = \frac{\sigma_2}{\sigma_0'}. \quad (13)$$

Substituting Eq. (11) into (13) leads to

$$\frac{\sigma_1^\infty}{\sigma_0}\sqrt{\frac{1}{r_1}} = \frac{\sigma_2^\infty}{\sigma_0'}\sqrt{\frac{1}{r_2}}. \quad (14)$$

Since the ratio of remote boundary stress to general strength is approximately a constant once the m value is determined [45], the ratios in the Eq. (14) can be eliminated, and thus we come to

$$r_1 = r_2. \quad (15)$$

Combing Eq. (10) with Eq. (14), one can obtain that the Mode I fracture toughness is also proportional to the general strength and come to the same conclusion as Eq. (15) formulated. Above theoretical analysis links the heterogeneity index to the FPZ size, confirms the dependence of the FPZ size on heterogeneity, and suggest that the FPZ size is not determined by either the tensile strength or Mode I fracture toughness.

As formulated in Eq. (1), the tensile strength and Mode I fracture toughness lie in the numerator and the denominator, and thus neither parameter is more important than the other to influence FPZ size. What is more important to the FPZ size is their ratio relationship. Since the tensile strength and fracture toughness are both proportional to general strength, and the proportionality coefficients are determined by m value [44,45], the ratio of tensile strength to fracture toughness can vary within a certain range (Fig. 9), which indicates that FPZ size has an upper limitation and the limitation may depend on the range of heterogeneity degree [46], because the heterogeneity of rocks cannot be infinite. This may explain why the FPZ size becomes approximately constant after specimen size increases to reach a certain level [11].

4.3 Implications of the FPZ size

The experiment and numerical simulation results suggest that specimens with strong heterogeneity generate greater number of micro cracks and exhibit more irregular crack morphology. As the theoretical analysis demonstrates, strong heterogeneity can raise the probability of cracking within a larger range at the vicinity of a crack tip, extending the FPZ. Since a large FPZ comprise a great number of micro cracks, the stress fields at the tips of Mode I cracks can be very complex owing to the interaction between the micro cracks; under this circumstance, macroscopic cracks consisting of the scattered micro cracks can propagate following curving even bifurcate paths, deviating from the direction as linear elastic fracture mechanics predicts.

Large FPZ of certain types of reservoir rock may imply that such rocks have strong fracability [47], i.e., they are suitable for conducting hydraulic fracturing. Great number of cracks can be generated when such rocks are stimulated by injected fluids, and the hydraulic fractures with curving morphology probably connect with more preexisting crack and pores, raising the conductivity of reservoirs. Therefore, optimization of designing hydraulic fracturing highly relies on reliable fracability evaluation of reservoir rocks. Uncovering the dependence of the FPZ size on heterogeneity can provide important guidelines for the fracability evaluation.

5. Conclusions

We conducted experiments and numerical simulations on rocks with different heterogeneities and showed that strong heterogeneity resulted in large FPZ size. The mechan-

ical mechanism behind this positive correlation is explained using the Weibull distribution and fracture mechanism, which shows that strong heterogeneity enhances the probability of cracking within a FPZ with large size, and the FPZ size is not determined by either tensile strength or fracture toughness.

Furthermore, nonlinear deformation involving generation of cracks can easily occur in heterogeneous rocks with large FPZs, which causes greater number of micro cracks and more complex crack morphology. The relationships between heterogeneity, FPZ size and crack morphology suggest that FPZ size may be useful for fracability evaluation of reservoir.

These findings can improve our recognition to the mechanical mechanism of Mode I crack propagation and the inherent rules it adheres to, and they show significant engineering implications in evaluation of reservoir fracability.

Author Contributions: Conceptualization, J.N. and H.C.; methodology, J.N., M.Z. and H.C.; validation, J.N.; formal analysis, H.C.; investigation, H.C., M.Z. and J.N.; resources, J.N.; writing—original draft preparation, H.C.; writing—review and editing, J.N., M.Z. and H.C.; visualization, H.C. and M.Z.; funding acquisition, J.N. and H.C. All authors have read and agreed to the published version of the manuscript.

Funding: This research was funded by the National Natural Science Foundation of China, grant numbers 42107184 and 41602330.

Data Availability Statement: All the data required to evaluate the conclusions of this study are present in the paper. The authors will provide additional data related to this paper upon request.

Conflicts of Interest: The authors declare no conflict of interest.

References

1. Lawn, B.R.; Wilshaw, T.R. *Fracture of brittle solids*; Cambridge University Press: New York, 1975.
2. Liu, G.; Chen, Y.; Du, X.; Wang, S.; Fernández-Steeger, T.M. Evolutionary analysis of heterogeneous granite microcracks based on digital image processing in grain-block model. *Materials* **2022**, *15*, 1941, doi:10.3390/ma15051941.
3. Lan, H.; Martin, C.D.; Hu, B. Effect of heterogeneity of brittle rock on micromechanical extensile behavior during compression loading. *J Geophys Res-Sol Ea* **2010**, *115*, doi:10.1029/2009JB006496.
4. Shirole, D.; Walton, G.; Hedayat, A. Experimental investigation of multi-scale strain-field heterogeneity in rocks. *Int J Rock Mech Min Sci* **2020**, *127*, 104212, doi:10.1016/j.ijrmms.2020.104212.
5. Atkinson, B.K. *Fracture mechanics of rock*; Academic Press: London, 1987.
6. Labuz, J.F.; Shah, S.P.; Dowding, C.H. Measurement and description of tensile fracture in granite. *J Eng Mech* **1989**, *115*, 1935-1949, doi:10.1061/(ASCE)0733-9399(1989)115:9(1935).
7. Moazzami, M.; Ayatollahi, M.; Akhavan-Safar, A. Assessment of the fracture process zone in rocks using digital image correlation technique: The role of mode-mixity, size, geometry and material. *Int J Damage Mech* **2020**, *29*, 646-666, doi:10.1177/1056789519871334.
8. Zietlow, W.K.; Labuz, J.F. Measurement of the intrinsic process zone in rock using acoustic emission. *Int J Rock Mech Min Sci* **1998**, *35*, 291-299, doi:10.1016/S0148-9062(97)00323-9.
9. Brooks, Z. Fracture process zone: Microstructure and nanomechanics in quasi-brittle materials. Dissertation of Doctor, Massachusetts Institute of Technology, Boston, 2013.
10. Fakhimi, A.; Tarokh, A. Process zone and size effect in fracture testing of rock. *Int J Rock Mech Min Sci* **2013**, *60*, 95-102, doi:10.1016/j.ijrmms.2012.12.044.
11. Tarokh, A.; Makhnenko, R.Y.; Fakhimi, A.; Labuz, J.F. Scaling of the fracture process zone in rock. *Int J Fract* **2017**, *204*, 191-204, doi:10.1007/s10704-016-0172-0.
12. Haidar, K.; Pijaudier-Cabot, G.; Dubé, J.F.; Loukili, A. Correlation between the internal length, the fracture process zone and size effect in model materials. *Mater Struct* **2005**, *38*, 201-210, doi:10.1007/BF02479345.

13. Guha Roy, D.; Singh, T.N.; Kodikara, J. Influence of joint anisotropy on the fracturing behavior of a sedimentary rock. *Eng Geol* **2017**, *228*, 224-237, doi:10.1016/j.enggeo.2017.08.016.
14. Han, Z.; Zhou, J.; Zhang, L. Influence of grain size heterogeneity and in-situ stress on the hydraulic fracturing process by PFC2D modeling. *Energies* **2018**, *11*, 1413, doi:10.3390/en11061413.
15. Tang, H.; Li, S.; Zhang, D. The effect of heterogeneity on hydraulic fracturing in shale. *J Pet Sci Eng* **2018**, *162*, 292-308, doi:10.1016/j.petrol.2017.12.020.
16. Yang, T.H.; Tham, L.G.; Tang, C.A.; Liang, Z.Z.; Tsui, Y. Influence of heterogeneity of mechanical properties on hydraulic fracturing in permeable rocks. *Rock Mech Rock Eng* **2004**, *37*, 251-275, doi:10.1007/s00603-003-0022-z.
17. Davraz, A.; Nalbantçılar, M.T.; Varol, S.; Önden, İ. Hydrogeochemistry and reservoir characterization of the Konya geothermal fields, Central Anatolia/Turkey. *Geochemistry* **2022**, *82*, 125867, doi:10.1016/j.chemer.2022.125867.
18. Gunes Yilmaz, N.; Karaca, Z.; Goktan, R.M.; Akal, C. Relative brittleness characterization of some selected granitic building stones: Influence of mineral grain size. *Constr Build Mater* **2009**, *23*, 370-375, doi:10.1016/j.conbuildmat.2007.11.014.
19. Li, X.; Marasteanu, M. The fracture process zone in asphalt mixture at low temperature. *Eng Fract Mech* **2010**, *77*, 1175-1190, doi:10.1016/j.engfracmech.2010.02.018.
20. Spagnoli, A.; Carpinteri, A.; Ferretti, D.; Vantadori, S. An experimental investigation on the quasi-brittle fracture of marble rocks. *Fatigue Fract Eng M* **2016**, *39*, 956-968, doi:10.1111/ffe.12429.
21. Erarslan, N. Microstructural investigation of subcritical crack propagation and Fracture Process Zone (FPZ) by the reduction of rock fracture toughness under cyclic loading. *Eng Geol* **2016**, *208*, 181-190, doi:10.1016/j.enggeo.2016.04.035.
22. ISRM Commission on standardization of laboratory and field tests. Suggested methods for determining tensile strength of rock materials. *Int J Rock Mech Min Sci Geomech Abstr* **1978**, *15*, 99-103, doi:10.1016/0148-9062(78)90003-7.
23. American Society of Testing Materials. Standard Test Method for Splitting Tensile Strength of Intact Rock Core Specimens. **2016**, *D3967 - 16*, 1-5, doi:10.1520/D3967-16.
24. Kuruppu, M.D.; Obara, Y.; Ayatollahi, M.R.; Chong, K.P.; Funatsu, T. ISRM-suggested method for determining the Mode I static fracture toughness using semi-circular bend specimen. *Rock Mech Rock Eng* **2014**, *47*, 267-274, doi:10.1007/s00603-013-0422-7.
25. ISRM Commission on standardization of laboratory and field tests. Suggested methods for determining the fracture-toughness of rock. *Int J Rock Mech Min Sci* **1988**, *25*, 71-96.
26. Fowell, R.J.; Xu, C.; Dowd, P.A. An update on the fracture toughness testing methods related to the cracked chevron-notched Brazilian disk (CCNBD) specimen. *Pure Appl Geophys* **2006**, *163*, 1047-1057, doi:10.1007/s00024-006-0057-7.
27. Potyondy, D.O.; Cundall, P.A. A bonded-particle model for rock. *Int J Rock Mech Min Sci* **2004**, *41*, 1329-1364, doi:10.1016/j.ijrmms.2004.09.011.
28. Han, Z.; Zhang, L.; Azzam, R.; Zhou, J.; Wang, S. A statistical index indicating the degree and mechanical effects of grain size heterogeneity in rocks. *Eng Geol* **2021**, *293*, 106292, doi:10.1016/j.enggeo.2021.106292.
29. Potyondy, D.O. A grain-based model for rock: approaching the true microstructure. In Proceedings of the Rock Mechanics in the Nordic Countries 2010, Kongsberg, Norway, 2010; pp. 225-234.
30. Zhou, J.; Lan, H.; Zhang, L.; Yang, D.; Song, J.; Wang, S. Novel grain-based model for simulation of brittle failure of Alxa porphyritic granite. *Eng Geol* **2019**, *251*, 100-114, doi:10.1016/j.enggeo.2019.02.005.
31. Itasca Consulting Group Inc. PFC2D—Particle Flow Code in 2 Dimensions. **2019**.
32. Zhai, M.; Xue, L.; Bu, F.; Yang, B.; Ding, H. Microcracking behaviors and acoustic emission characteristics of granite subjected to direct shear based on a novel grain-based model. *Computers and Geotechnics* **2022**, *151*, 104955, doi:10.1016/j.compgeo.2022.104955.
33. Pierce, M.; Cundall, P.; Potyondy, D.; Ivars, D.M. A synthetic rock mass model for jointed rock. In Proceedings of the 1st Canada - U.S. Rock Mechanics Symposium, 2007.

34. Schön, J.H. *Physical properties of rocks : Fundamentals and principles of petrophysics (second edition)*; Elsevier: Amsterdam, 2015; Volume 65.
35. Bahrani, N.; Kaiser, P.K.; Valley, B. Distinct element method simulation of an analogue for a highly interlocked, non-persistently jointed rockmass. *Int J Rock Mech Min Sci* **2014**, *71*, 117-130, doi:10.1016/j.ijrmms.2014.07.005.
36. Niu, J. Research on the fracture mechanics index of rock fracability evaluation. Dissertation of Doctor, University of Chinese Academy of Sciences, Beijing, 2015.
37. Wong, L.N.Y.; Einstein, H.H. Crack coalescence in molded gypsum and Carrara marble: Part 2—Microscopic observations and interpretation. *Rock Mech Rock Eng* **2009**, *42*, 513-545, doi:10.1007/s00603-008-0003-3.
38. Morgan, S.P.; Johnson, C.A.; Einstein, H.H. Cracking processes in Barre granite: fracture process zones and crack coalescence. *Int J Fract* **2013**, *180*, 177-204, doi:10.1007/s10704-013-9810-y.
39. Cesano, D.; Bagtzoglou, A.C.; Olofsson, B. Quantifying fractured rock hydraulic heterogeneity and groundwater inflow prediction in underground excavations: the heterogeneity index. *Tunn Undergr Sp Tech* **2003**, *18*, 19-34, doi:10.1016/S0886-7798(02)00098-6.
40. Sabri, M.; Ghazvinian, A.; Nejati, H.R. Effect of particle size heterogeneity on fracture toughness and failure mechanism of rocks. *Int J Rock Mech Min Sci* **2016**, *81*, 79-85, doi:10.1016/j.ijrmms.2015.11.002.
41. Mahabadi, O.K.; Tatone, B.S.A.; Grasselli, G. Influence of microscale heterogeneity and microstructure on the tensile behavior of crystalline rocks. *J Geophys Res-Sol Ea* **2014**, *119*, 5324-5341, doi:10.1002/2014JB011064.
42. Weibull, W. A statistical distribution function of wide applicability. *J Appl Mech* **1951**, *13*, 293-297.
43. Tang, C.A.; Liu, H.; Lee, P.K.K.; Tsui, Y.; Tham, L.G. Numerical studies of the influence of microstructure on rock failure in uniaxial compression — Part I: effect of heterogeneity. *Int J Rock Mech Min Sci* **2000**, *37*, 555-569, doi:10.1016/S1365-1609(99)00121-5.
44. Liu, H.Y.; Roquete, M.; Kou, S.Q.; Lindqvist, P.A. Characterization of rock heterogeneity and numerical verification. *Eng Geol* **2004**, *72*, 89-119, doi:10.1016/j.enggeo.2003.06.004.
45. Zhu, W.; Tang, C.a. Micromechanical model for simulating the fracture process of rock. *Rock Mech Rock Eng* **2004**, *37*, 25-56, doi:10.1007/s00603-003-0014-z.
46. Yang, B.C.; Qin, S.Q.; Xue, L.; Chen, H.R. The reasonable range limit of the shape parameter in the Weibull distribution for describing the brittle failure behavior of rocks. *Rock Mech Rock Eng* **2021**, *54*, 3359-3367, doi:10.1007/s00603-021-02414-1.
47. Meng, F.; Wong, L.N.Y.; Zhou, H. Rock brittleness indices and their applications to different fields of rock engineering: A review. *J Rock Mech Geotech Eng* **2021**, *13*, 221-247, doi:10.1016/j.jrmge.2020.06.008.